The Plant Cell, Vol. 25: 3988–3999, October 2013, www.plantcell.org

Neighboring Parenchyma Cells Contribute to *Arabidopsis* Xylem Lignification, while Lignification of Interfascicular Fibers Is Cell Autonomous[W]

Rebecca A. Smith,[a,b,1] Mathias Schuetz,[a,b,1] Melissa Roach,[c] Shawn D. Mansfield,[c] Brian Ellis,[b] and Lacey Samuels[a,2]

[a] Department of Botany, University of British Columbia, Vancouver, British Columbia V6T 1Z4, Canada
[b] Michael Smith Laboratories, University of British Columbia, Vancouver, British Columbia V6T 1Z4, Canada
[c] Department of Wood Science, University of British Columbia, Vancouver, British Columbia V6T 1Z4, Canada

ORCID ID: 0000-0002-0606-8933 (L.S.).

Lignin is a critical structural component of plants, providing vascular integrity and mechanical strength. Lignin precursors (monolignols) must be exported to the extracellular matrix where random oxidative coupling produces a complex lignin polymer. The objectives of this study were twofold: to determine the timing of lignification with respect to programmed cell death and to test if nonlignifying xylary parenchyma cells can contribute to the lignification of tracheary elements and fibers. This study demonstrates that lignin deposition is not exclusively a postmortem event, but also occurs prior to programmed cell death. Radiolabeled monolignols were not detected in the cytoplasm or vacuoles of tracheary elements or neighbors. To experimentally define which cells in lignifying tissues contribute to lignification in intact plants, a microRNA against *CINNAMOYL CoA-REDUCTASE1* driven by the promoter from *CELLULOSE SYNTHASE7* (*ProCESA7:miRNA CCR1*) was used to silence monolignol biosynthesis specifically in cells developing lignified secondary cell walls. When monolignol biosynthesis in *ProCESA7:miRNA CCR1* lines was silenced in the lignifying cells themselves, but not in the neighboring cells, lignin was still deposited in the xylem secondary cell walls. Surprisingly, a dramatic reduction in cell wall lignification of extraxylary fiber cells demonstrates that extraxylary fibers undergo cell autonomous lignification.

INTRODUCTION

Plants in terrestrial environments accumulate substantial biomass and size due to the evolution of lignified cells that transport water and minerals and provide structural support for upright growing stems. Lignin is the complex phenolic polymer that strengthens the secondary cell wall of xylem cells, such as water-conducting tracheary elements and supportive fibers, and is most evident in woody tissues of trees. Studies of lignin biosynthesis and degradation are at the forefront of plant cell wall research because of its importance in plant structure and function and also because of the major difficulties associated with its removal during industrial processing for a range of products, including wood pulp and biofuels from plant tissues. The biosynthesis of lignin precursors, termed monolignols, occurs through the phenylpropanoid pathway and is relatively well understood (Humphreys and Chapple, 2002; Vanholme et al., 2010), but little is known about how monolignols are exported from their site of synthesis inside the cell to the specific cell wall domains where they polymerize (Liu et al., 2011; Sibout and Höfte, 2012).

The development of lignified cells is the result of a series of overlapping events, including cell morphogenesis, secondary cell wall deposition (cellulose/hemicellulose), lignification, and programmed cell death. Following cell expansion, deposition of the cellulose and hemicellulose polysaccharides in the secondary cell wall requires living cells with intact protoplasts. In a wide variety of species, monolignol deposition appears to overlap with polysaccharide deposition during cell development, suggesting that lignification begins prior to programmed cell death (Pickett-Heaps, 1968; Takabe et al., 1985; Terashima et al., 1986, 1993; Terashima and Fukushima, 1988; Roberts et al., 2004). In xylem cell culture systems, lignification of tracheary element cell walls continues to increase after tracheary element cell death (Hosokawa et al., 2001), and pharmacological inhibition of cell death stopped lignification (Pesquet et al., 2013). As the earlier studies employed chemical fixation protocols where lignin precursors could have migrated during sample processing, and cell culture studies lack the whole tissue context, one goal of this study was to use cryofixation of intact *Arabidopsis thaliana* roots to determine the precise timing of lignification relative to programmed cell death and the spatial distribution of monolignols in tracheary elements.

The demonstration of postmortem lignification in cell cultures has led to the establishment of the "good neighbor" hypothesis, wherein nonlignified cells adjacent to lignifying cells may be synthesizing monolignols and exporting them to the lignified cell walls for polymerization (Hosokawa et al., 2001; Tokunaga et al., 2005; Pesquet et al., 2013). The good neighbor lignification model is indirectly supported by the fact that monolignol biosynthetic

[1] These authors contributed equally to this work.
[2] Address correspondence to lsamuels@mail.ubc.ca.
The author responsible for distribution of materials integral to the findings presented in this article in accordance with the policy described in the Instructions for Authors (www.plantcell.org) is: Lacey Samuels (lsamuels@mail.ubc.ca).
[W] Online version contains Web-only data.
www.plantcell.org/cgi/doi/10.1105/tpc.113.117176

gene expression is prevalent in nonlignifying neighboring cells adjacent to lignifying xylem cell types in *Arabidopsis*, tobacco (*Nicotiana tabacum*), and poplar (*Populus trichocarpa*) plants (Bevan et al., 1989; Hauffe et al., 1991; Feuillet et al., 1995; Chen et al., 2000; Baghdady et al., 2006). The good neighbor hypothesis was developed based on studies of *Zinnia elegans* and *Arabidopsis* tracheary element cell cultures, but within intact plants tracheary elements represent only a small subset of cells with thick lignified secondary cell walls. Fiber cells, for example, play a critical role in load bearing and are a main component of woody biomass, yet the mechanisms of their lignification are not modeled by existing cell culture systems.

The objectives of this study were to examine both the timing of lignification and spatial distribution of monolignols, using autoradiography of tracheary elements in intact tissues, and to directly test the good neighbor hypothesis by reducing monolignol production in a variety of cell types with thick secondary cell walls and assessing whether nonlignifying neighbors can compensate. The promoter of the secondary wall *CELLULOSE SYNTHASE7*/*IRREGULAR XYLEM3* (*CESA7*/*IRX3*) gene, which is expressed both in tracheary elements and fibers (Taylor et al., 1999, 2003; Mitsuda et al., 2007; McDonnell, 2010), was used to drive the expression of a silencing microRNA that targets an essential monolignol biosynthetic gene, *CINNAMOYL CoA REDUCTASE1* (*CCR1*) (Jones et al., 2001). The targeted silencing of monolignol biosynthesis in *proCESA7*:*miRNA CCR1* plants did not result in lignin defects in the xylem tissues, whereas supportive fibers outside of the xylem tissue in these plants had little lignin. Thus, both tracheary elements and xylary fibers appear to have good neighbors, while the structural fibers outside the vascular bundles employ an autonomous lignification mechanism.

RESULTS

Monolignols Are Deposited before and just after Programmed Cell Death in TE

While the majority of lignification in xylem cell cultures is considered a postmortem event (Hosokawa et al., 2001; Pesquet et al., 2010, 2013), lignin deposition in intact developing xylem in woody plants occurs extensively before, as well as after, programmed cell death (Terashima et al., 1986; Terashima and Fukushima, 1988; Kaneda et al., 2008). To visualize both cell death and lignification in primary xylem development in situ, lignin was labeled in *Arabidopsis* seedling roots using the radiolabeled precursor of monolignols, tritiated Phe (^{3}H-Phe). Whole seedlings were incubated for 2 h in media containing ^{3}H-Phe and then high-pressure frozen to immobilize radiolabeled metabolites in situ. Autoradiography was then used to examine incorporation of radiolabel into tracheary element secondary cell walls as a consequence of de novo lignin biosynthesis. To restrict ^{3}H-Phe metabolism to phenylpropanoid biosynthesis, cycloheximide, an inhibitor of protein translation, was incubated with ^{3}H-Phe. Following sectioning, the cellular distribution of label was evaluated by microautoradiography. Living, developing protoxylem tracheary elements were identified in corresponding reference sections based on the observation of intact vacuoles and cellular contents (Figure 1A). Autoradiographic sections of control roots treated with ^{3}H-Phe alone for 2 h were labeled throughout the cytoplasm of all cell types (see Supplemental Figures 1A and 1B online), while in ^{3}H-Phe and cycloheximide-treated roots, label was restricted to the spiral wall thickenings of the protoxylem tracheary elements and to the periphery of cells in the cortex (Figures 1A to 1C). When ^{3}H-Phe was supplied together with the general phenylpropanoid pathway inhibitor piperonylic acid (Chong et al., 2001), the tracheary element cell wall label was abolished (see Supplemental Figures 1C and 1D online), as expected if the cell wall label is lignin.

Longitudinal sections of roots were mapped with the distribution of radioactively labeled phenylpropanoids from the root tip, where little radioactivity was incorporated in the cycloheximide-treated samples, along the xylem developmental gradient (Figure 1C). Following the 2-h pulse of radiolabel into the developing xylem, living tracheary elements, as well as tracheary elements with no visible cytoplasmic contents were observed. Of 54 labeled developing tracheary elements observed in the correct developmental stage and plane of section, 18 were living and 36 were dead. Living tracheary elements, or recently dead tracheary elements, had much stronger radiolabel in the cell wall compared with the label in the cell walls of older dead tracheary elements (Figures 1B and 1C). Mature xylem cells distal from the root tip were not labeled during the exposure period (Figure 1C).

In contrast with the strong label that appeared in the cell wall/cell periphery, the amount of label present inside the cytoplasm of all cells was at background levels, even after extended exposure (2 to 3 weeks) of the silver emulsion to the sample. To determine whether the distribution of radiolabel specifically overlapped with the secondary cell wall domains, it was necessary to use autoradiography coupled to transmission electron microscopy (TEM) to provide higher resolution. In reference TEM sections examined prior to performing autoradiography, living tracheary elements with an intact central vacuole, cytoplasm, and spiral cell wall thickenings were routinely observed (Figure 2A). After autoradiography of samples treated with ^{3}H-Phe and cycloheximide, strong distribution of radiolabel was observed in the secondary cell walls (Figures 2B and 2C). In contrast with the wall label, the levels of radiolabel within the cell were at background. This limited intracellular labeling suggests that the cytoplasmic pool of monolignols and intermediates in the pathway leading from Phe to monolignol synthesis is very small, consistent with a high flux of phenylpropanoid metabolism. The strong labeling observed in the walls of cells with intact cytoplasm indicates that lignification is not exclusively a postmortem event in its normal developmental context because there is substantial deposition of monolignols/lignin while the lignifying cell is still alive.

The weaker, but significant, label detected in dead tracheary elements (Figures 1B and 1C) confirms the cell culture finding that the lignification of secondary cell walls can continue postmortem (Hosokawa et al., 2001; Pesquet et al., 2013). With autoradiography, there was no evidence that monolignols accumulated within the vacuole before release to the cell wall for polymerization in primary xylem (Figure 2B). Consistent with the low vacuolar label, previous studies have reported undetectable levels of monolignols when soluble phenolics extracted from roots were

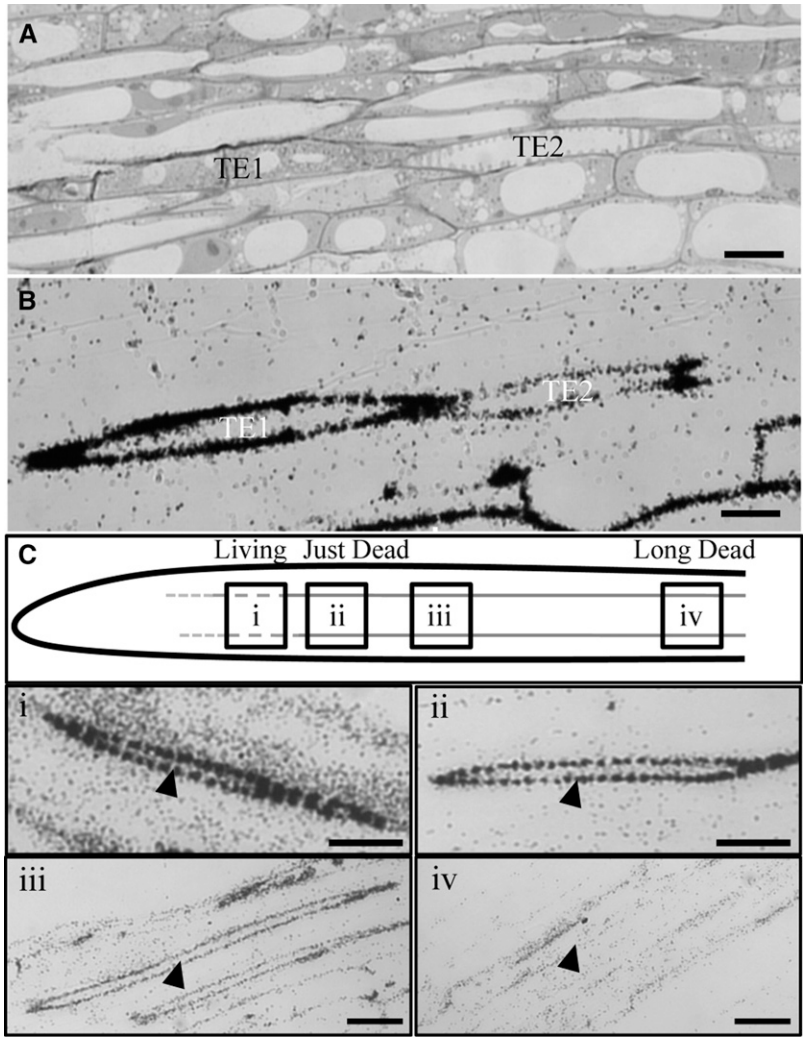

Figure 1. Secondary Cell Walls of *Arabidopsis* Tracheary Elements in Roots Undergo Lignification before Cell Death.

(A) *Arabidopsis* (Col-0) radiolabeled root section stained with Toluidine Blue through the late elongation zone, showing a living, lignifying tracheary element (TE1) and a dead, lignified tracheary element (TE2).

(B) Autoradiograph of an adjacent ^{3}H-Phe– and cycloheximide-treated root section with dark deposits where radiolabeled phenylpropanoids are localized.

(C) Model of the primary root developmental gradient showing differences in the amount of radiolabel incorporated in secondary cell walls of tracheary elements (red lines) during the 2-h incubation period and representative autoradiographic images along the developmental gradient, showing tracheary elements (arrowheads) with either (i) strong label in living TEs, (ii) strong label in TEs that have just undergone PCD, (iii) less label in slightly older TEs, or (iv) no/background label in TEs that are long dead.

Bars = 10 μm in **(A)** and **(B)** and 15 μm in **(C)**.

analyzed by HPLC (Hemm et al., 2004; Bednarek et al., 2005; Lanot et al., 2006). To test if vacuolar label was lost during high-pressure freezing and subsequent processing, nonlignifying cortical root cells outside the vascular region were used as an internal positive control. In contrast with developing tracheary elements, and their immediate neighbors, radiolabel of vacuolar phenolic contents was above background in cortical cells (see Supplemental Figure 1E online). If monolignols are not accumulating in vacuoles, but are deposited in cell walls both prior to and after programmed cell death in intact plants, then the question of whether lignifying cells themselves or neighboring cells, or both, supply lignin precursors is important.

Lignin Deposition Is Blocked by Constitutive Silencing of CCR

To directly test the contribution of secondary cell wall–forming cells toward their own lignification, monolignol biosynthesis was silenced in tracheary elements and fibers. First, an artificial microRNA (miRNA) was designed to target the key *Arabidopsis*

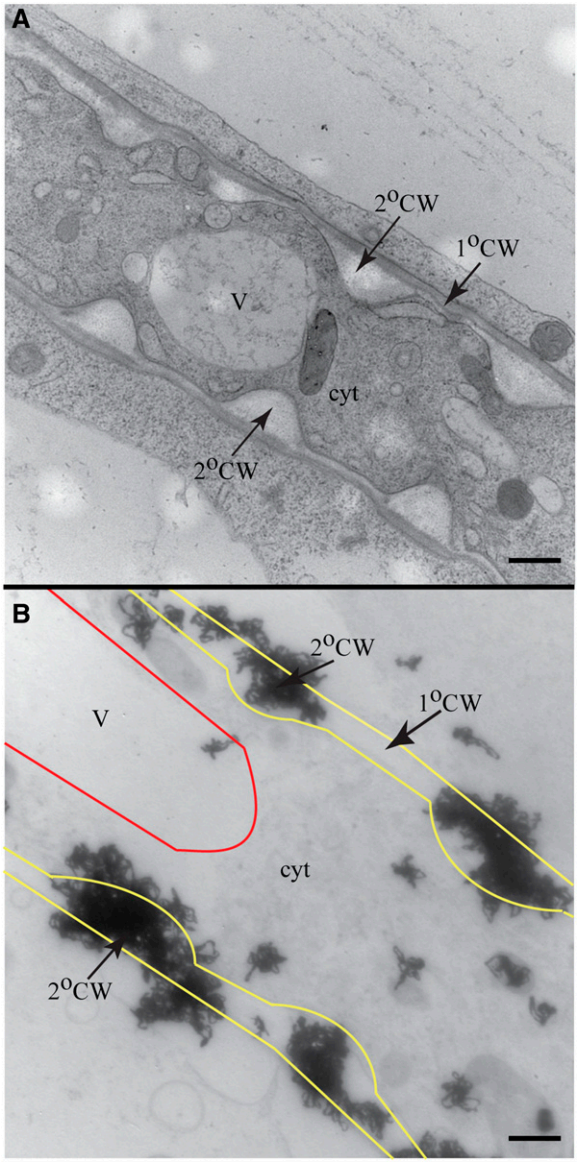

Figure 2. Monolignols Do Not Accumulate within Vacuoles or Cytoplasm of Root Tracheary Elements during Lignification.

(A) TEM image of living tracheary element with secondary cell wall thickenings.

(B) TEM autoradiograph with outlines superimposed over the vacuole (red) and plasma membrane (yellow) of a ^{3}H-Phe– and cycloheximide-treated living tracheary element. Dense label was found at secondary cell wall thickenings but not in the cytosol or vacuole.

V, vacuole; cyt, cytosol; 2°CW, secondary cell wall; 1°CW, primary cell wall. Bars = 500 nm.

monolignol biosynthesis gene, *CCR1* (Jones et al., 2001). The effectiveness of the miRNA in silencing *CCR1* was verified by driving expression of the *CCR1 miRNA* with the constitutive cauliflower mosaic virus *35S* promoter. *Arabidopsis Pro35S:miRNA CCR1* plants phenocopied previously described lignin-deficient mutants, including *ccr1* loss-of-function mutants (Jones et al., 2001; Mir Derikvand et al., 2008). Basic fuchsin, which is a fluorescent stain that binds to lignin, was used to assess lignification in tracheary elements of roots. In contrast with the lignified spiral wall thickenings of the protoxylem of wild-type roots (Figure 3A), little to no staining was observed of *Pro35S:miRNA CCR1* plants (Figure 3C), although secondary cell wall thickenings were observed in these lignin-deficient roots (Figure 3B).

Lignin Is Still Deposited in Root Protoxylem with Silencing of CCR Targeted to TE

To drive the expression of the *CCR1 miRNA* specifically in lignifying cell types, *CCR1 miRNA* expression was placed under the control of the secondary cell wall *CESA7* promoter. The tissue specificity of this promoter was demonstrated by analysis of *ProCESA7:GFP* plants, where green fluorescent protein (GFP) fluorescence was effectively restricted to cells undergoing secondary cell wall deposition in both roots (Figure 3D) and inflorescence stems (see Supplemental Figure 2 online; Taylor et al., 2003; Mitsuda et al., 2007; McDonnell, 2010).

In roots expressing the *ProCESA7:miRNA CCR1* construct, basic fuchsin staining showed that lignification of the xylem was indistinguishable from that observed in wild-type roots (Figure 3E). This result indicates that, in the absence of endogenous monolignol production in protoxylem tracheary elements, neighboring cells in the root are capable of contributing to the lignification of the secondary cell walls in those tracheary elements.

If the *CCR1 miRNA* was mobile and had spread from the tracheary elements where it was being expressed to adjacent neighbor cells, then *CCR1* silencing in these neighbor cells might have led to a reduced lignin phenotype similar to that of *Pro35S:miRNA CCR* roots, but this was not observed. Artificial miRNAs derived from the endogenous miRNA319 have limited mobility when expressed in a cell-specific manner (Schwab et al., 2006). This conclusion is supported by several other studies demonstrating that miRNAs have limited ability to spread to neighboring cells, in contrast with the systemic spread of short interfering RNA (reviewed in Ossowski et al., 2008). To confirm that *CCR1* silencing had occurred only in cells with active expression of *ProCesA7:miRNA CCR1*, the *CCR1 miRNA* plants were crossed with plants constitutively expressing a yellow fluorescent protein (YFP)–tagged CCR1 (*ProUBQ10:YFP-CCR1*), which showed strong *YFP-CCR1* expression in all cell types (Figure 4A). We postulated that the *CCR1* miRNA would silence both the endogenous *CCR1* and the *YFP-CCR1* translational fusion construct. The ability of the *CCR1 miRNA* to silence CCR1 was first tested by constitutively expressing *Pro35S:miRNA CCR1* together with *YFP-CCR1*, and the effect on the YFP-CCR1 signal was documented using confocal laser scanning microscopy. In the presence of *Pro35S:miRNA CCR1*, YFP fluorescence was barely detectable (see Supplemental Figure 3 online). However, when the *ProCesA7:miRNA CCR1* was expressed in the *YFP-CCR1* lines, strong expression of YFP-CCR1 was observed in cells neighboring the tracheary cells but not in living tracheary elements undergoing secondary cell wall deposition, such as the tracheary elements in primary roots (Figure 4B) and stems (see Supplemental Figure 4 online). To ensure that the loss of YFP-CCR1 signal reflected miRNA-targeted degradation of CCR

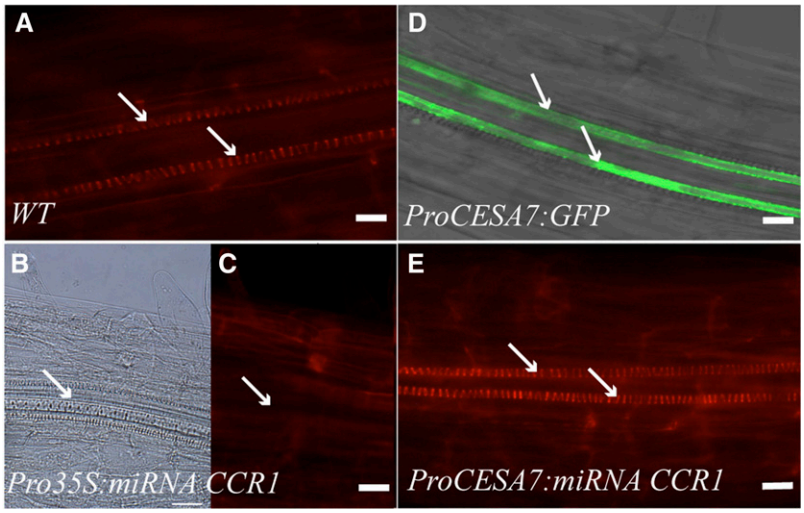

Figure 3. Neighboring Cells Can Rescue Tracheary Element Lignification in *Arabidopsis* Roots.

(A) Wild-type (WT) root stained with basic fuchsin shows well lignified tracheary elements (arrow).
(B) *Pro35S:miRNA CCR1*-expressing roots still develop tracheary elements (arrows).
(C) In *Pro35S:miRNA CCR1*, no fluorescence above background is observed in the areas of the tracheary elements (arrow).
(D) Tracheary elements (arrow) are the only cell types labeled in the late elongation zone by expression of *ProCESA7:GFP*.
(E) If downregulation of monolignol biosynthesis is restricted to tracheary elements by expression of tracheary element–specific *ProCESA7:miRNA CCR1*, basic fuchsin stain indicates lignification similar to the wild type.
Bars = 10 μm.

transcripts, rather than programmed cell death, developmentally matched samples were examined using the developing tracheary element most proximal to the root tip.

Lignin Deposition Is Decreased in Interfascicular Fibers but Not in the Xylem of Plants Expressing mIRNA CCR Driven by CesA7 Promoter

While roots of *Pro35S:miRNA CCR1* plants did not appear to have obvious morphological or developmental defects, the aerial portions of the plants displayed a semidwarf growth habit, with inflorescence stems that were thinner, highly flexible, and pendant (Figure 5). These plants also displayed fertility defects as previously described for genetic *ccr1* mutants (Jones et al., 2001; Thévenin et al., 2011). Quantitative RT-PCR analysis confirmed severely reduced or absent *CCR1* expression in these plants (see Supplemental Figure 5 online). Phloroglucinol staining of lignin in cross sections of inflorescence stems revealed the typical intense red stain of secondary cell walls in the wild type (Figures 6A and 6B). By contrast, *Pro35S:miRNA CCR1* lines had only low levels of lignin in tracheary elements, xylary fibers, and interfascicular fibers (Figures 6C and 6D). In addition, collapsed tracheary elements were observed in the xylem (irregular xylem phenotype), a phenomenon frequently observed in plants with defects in secondary cell wall formation or lignification (Turner and Somerville, 1997; Jones et al., 2001) (Figure 6C, arrows).

In the stem, the effect of silencing monolignol production using the *ProCESA7:miRNA CCR1* construct was particularly striking because secondary cell walls of cells from different tissues were affected differently (Figures 6E and 6F). Phloroglucinol staining of inflorescence stem sections from *ProCESA7:miRNA CCR1* plants revealed that lignified cells within the xylem, such as tracheary elements and xylary fibers, appeared normal and displayed wild-type levels of lignification, whereas the interfascicular fibers between the vascular bundles displayed drastic reductions in lignification (Figure 6E). Quantification of Klason acid–insoluble lignin confirmed this pattern. Stems of *Pro35S:miRNA CCR1* plants had the strongest reduction in lignin, with 37 to 49% of wild-type lignin levels. Stems of *ProCESA7:miRNA CCR1* had intermediate lignin levels, with 57 to 73% of wild-type lignin (Table 1). The monolignol composition of the *ProCESA7:miRNA CCR1* lignin exhibited minor changes, as thioacidolysis revealed slightly higher levels of S-units and reduced levels of G-units than in wild-type stems (see Supplemental Table 1 online), as observed in other lignin-deficient plants (Berthet et al., 2011; Thévenin et al., 2011). The specific decrease in interfascicular fiber lignification in *ProCESA7:miRNA CCR1* plants was correlated with a macroscopic stem phenotype where stems were more pendant and flexible than wild-type stems, although in contrast with the *Pro35S:miRNA CCR1* plants, the transgenic *ProCESA7:miRNA CCR1* plants appeared normal in height, growth, and fertility (Figure 5). Quantitative RT-PCR confirmed a decrease in *CCR1* expression in *ProCESA7:miRNA CCR1* plants compared with the wild type, but *CCR1 miRNA* transcript levels were not as dramatically decreased as the *Pro35S:miRNA CCR1* (see Supplemental Figure 5 online).

To establish which xylem cell types could potentially act as neighbors during lignification, inflorescence stem sections were examined using light microscopy and high-resolution TEM. Xylem parenchyma cells are interspersed among the tracheary elements and fibers of the vascular bundle (Figure 7) and are marked by their thin primary cell wall and the presence of

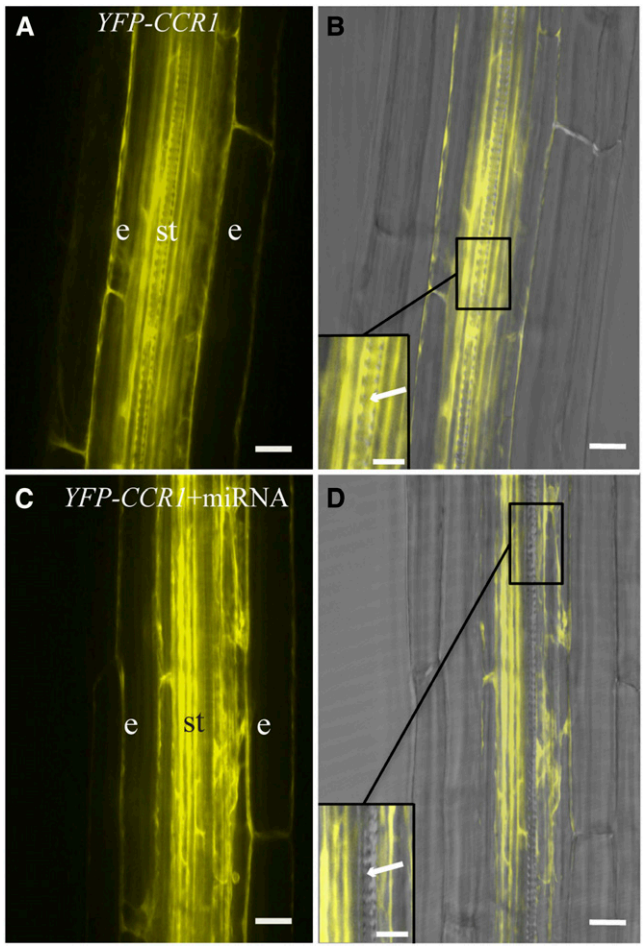

Figure 4. Cell-Specific Silencing of *CCR1* in *Arabidopsis* Roots.

(A) Fluorescence image of the developing stele of wild-type *Arabidopsis* roots expressing *ProUBQ10*:*YFP-CCR1*. e, endodermis; st, stele.
(B) Fluorescence image overlayed with corresponding bright-field image. YFP signal is observed in the late elongation zone of roots in endodermis and throughout the stele, including tracheary elements, which can be identified by their cell wall pattern (inset, arrow).
(C) Fluorescence image of YFP-CCR1 in the *ProCesA7*:*miRNA CCR1* plant lines.
(D) Fluorescence image overlayed with corresponding bright-field image. CCR1 is still expressed in endodermis and stele, but not in the tracheary elements (arrow, inset).
Bars = 150 μm in **(A)** to **(D)** and 75 μm in the insets.

persistent cytoplasmic contents, indicative of metabolically functional cells. By contrast, no parenchyma cells are interspersed among the interfascicular fibers outside the xylem, which were unable to lignify when their autonomous monolignol production was suppressed through *CCR1* silencing.

DISCUSSION

The first objective of this study was to determine the spatial distribution and timing of lignification by examining the cellular context for lignin deposition mechanisms in intact *Arabidopsis* roots. Cryofixation/autoradiography revealed that lignification in intact primary xylem occurs prior to programmed cell death, as well as continuing postmortem, as predicted by cell culture systems (Hosokawa, et al., 2001; Pesquet et al., 2013). The second objective was to test the good neighbor hypothesis. By reducing monolignol biosynthesis only in cells with thickened secondary cells walls, diverse mechanisms of monolignol contributions in the xylem were distinguishable from those operating in the supportive fibers outside of the vascular bundles.

Cryofixation coupled with autoradiography revealed the in situ distribution of phenylpropanoid metabolites in developing xylem (Figure 1). From these data, two conclusions can be inferred: First, lignification precedes and overlaps with programmed cell death; second, phenylpropanoids move rapidly through lignifying tissues and are rapidly concentrated in secondary cell walls, suggesting that monolignols or monolignol glucosides do not accumulate inside cells. Only background signals were detected in the cytoplasm of both lignifying cells and their nonlignifying

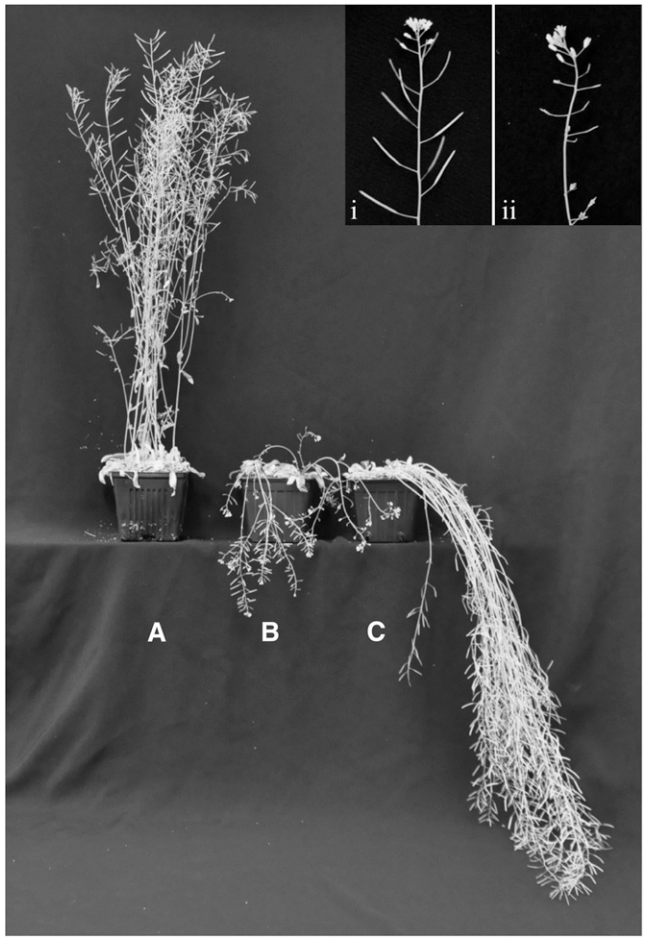

Figure 5. Stem Phenotypes of the miRNA-Expressing Plants.

Growth habit of 2-month-old wild-type and miRNA plants. The wild type **(A)**, *Pro35S*:*miRNA CCR1* **(B)**, and *ProCESA7*:*miRNA CCR1* **(C)**. Inset is a close-up of a wild-type inflorescence stem with normal siliques (i) and a *Pro35S*:*miRNA CCR1* inflorescence stem showing fertility defects (ii).

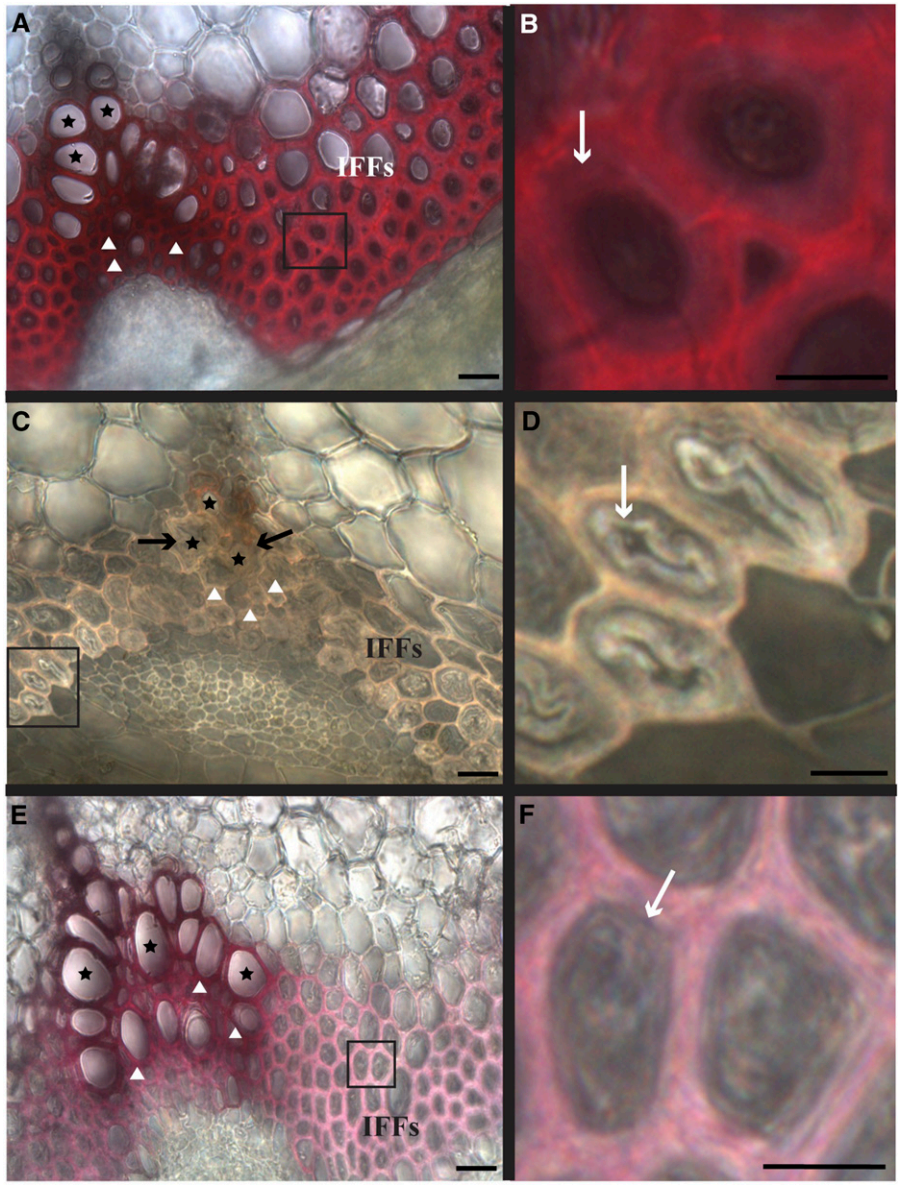

Figure 6. *Arabidopsis* Stem Tissues Show Diverse Degrees of Cell-Autonomous Lignification.

(A) *Arabidopsis* stem cross section (wild type) stained with phloroglucinol-HCl. IFF, interfascicular fibers.
(B) Enlargement of wild-type interfascicular fibers shown in **(A)**, with secondary cell wall thickenings (white arrow).
(C) Loss of stem lignification in all cell types demonstrated with low phloroglucinol-HCl staining when monolignol biosynthesis is knocked down with *Pro35S*:*miRNA CCR1*; arrows indicate collapsed tracheary elements.
(D) Enlargement of the interfascicular fibers shown in **(C)**, where the inner secondary cell wall layers (arrow) detach in these miRNA lines.
(E) When monolignol biosynthesis is downregulated in cells with thickened secondary cell walls using *ProCesA7*:*miRNA CCR1* line A, the vascular bundles of the stem still stained with phloroglucinol-HCl, while interfascicular fibers did not.
(F) Enlargement of the interfascicular fibers shown in **(E)**, where the secondary cell wall thickenings remain intact (arrow).
Stars indicate tracheary element; triangles indicate xylary fibers. Bars = 15 μm in **(A)**, **(C)**, and **(E)** and 5 μm in **(B)**, **(D)**, and **(F)**.

neighbors, indicating that the synthesis and transport of monolignols in these cells must be rapid (Figure 2). There also was no evidence of vacuolar or endomembrane accumulation of monolignols in developing xylem cells prior to programmed cell death. Accumulation of monolignol glucosides in the vacuole, followed by monolignol release during protoplast lysis, has been hypothesized as a lignification mechanism (Leinhos and Savidge, 1993; Pesquet et al., 2010). However, a recent study in *Arabidopsis* characterized the β-glucosidases with activity against monolignol glucosides and demonstrated that while

Table 1. Chemical Analysis of Lignin in Different miRNA Lines

Plant	Klason (Acid-Insoluble) Lignin (mg/100 mg Dry Cell Walls ± SD)	Acid-Soluble Lignin (mg/100 mg Dry Cell Walls ± SD)
The wild type (Col-0)	19.58 ± 0.19 (100)	2.09 ± 0.13
Pro35S:CCR miRNA line A	7.30 ± 0.17 (37)	3.57 ± 0.08
Pro35S:CCR miRNA line B	9.66 ± 0.03 (49)	3.38 ± 0.04
ProCESA7:CCR miRNA line A	11.22 ± 0.03 (57)	2.46 ± 0.08
ProCESA7:CCR miRNA line B	14.35 ± 0.24 (73)	2.02 ± 0.04

their loss of function influenced coniferin and coniferyl alcohol pools, it did not change lignification, suggesting that monolignol glucosides are not the direct precursors of lignin (Chapelle et al., 2012). These results are consistent with a previous autoradiographic study from developing pine wood where ^{3}H-Phe products were strongly detected in the cell wall but neither in vacuoles, as assessed by microscopy, nor in the extractable phenolic pool when monitored by HPLC and scintillation counting (Kaneda et al., 2008). These data support a lignification model where monolignols are rapidly exported across the plasma membrane for cross-linking in the cell wall. This rapid export is most likely facilitated by ABC transporters in the plasma membrane (Miao and Liu, 2010; Alejandro et al., 2012). The direct use of monolignols, and not monolignol glucosides, in lignification is also supported by another lignification model system, the Casparian strip in the endodermis of roots, in which lignification occurs gradually and without prior accumulation of monolignols (Naseer et al., 2012; Lee et al., 2013). Furthermore, xylary parenchyma cells may not be the only good neighbors in xylem tissues, as our data do not exclude the possibility that long-lived xylary fibers may also contribute to tracheary element lignification.

The targeted downregulation of monolignol biosynthesis permitted direct experimental testing of the good neighbor hypothesis (i.e., that nonlignified metabolically active cells participate in lignification of neighboring cells). Expression of *ProCESA7:miRNA CCR1* specifically in cells with thickened cell walls effectively silenced *CCR1* expression in these cells (Figure 4), yet xylem cells were still able to lignify their secondary cell walls (Figures 3 and 6). By contrast, lignification of the interfascicular fibers was strongly reduced, as demonstrated spatially by phloroglucinol staining and quantitatively by Klason analysis (Table 1). These two contrasting cell populations, xylem and lignifying interfascicular fibers, are specified by different transcriptional networks regulated by *VASCULAR NAC-DOMAIN* (*VND*) and *SECONDARY WALL-ASSOCIATED NAC DOMAIN1* (*SND1*) transcription factors, respectively (Kubo et al., 2005; Zhong et al., 2010). In poplar wood, these two cell populations display different lignin chemistry, depending on their proximity to one another (Gorzsás et al., 2011). In addition, developmentally non-cell-autonomous lignification in xylem tissues is consistent with tracheary elements undergoing programmed cell death, the final stage in their development, much earlier than fibers (Courtois-Moreau et al., 2009). Perhaps it is not surprising that these tissues have distinct lignification mechanisms, given their diverse transcriptional networks and the developmental differences between them.

A recent study (Yang et al., 2013) exploited the different transcriptional networks in xylem versus extraxylary fibers and used the promoter for a key VND transcription factor to rescue lignification only in xylem tissues by expression of *ProVND6:C4H* in the *c4h*^{ref3} background. The resulting stem phenotype appeared identical to that observed in the *ProCESA7:miRNA CCR1* stems. Although the stem phenotype described by Yang et al. (2013) and this study appear identical, the conclusions that can be drawn about lignification are different. The *VND6* promoter, unlike the *CESA7* promoter, has a broad expression pattern in *Arabidopsis* stem xylem and is expressed in all xylem cell types, with or without secondary cell walls (Yamaguchi et al., 2010a). The activity of VND transcription factors, such as VND6, may be posttranslationally restricted to xylem vessels by interaction with VND-INTERACTING2, which is expressed in xylary parenchyma cells and functions as a transcriptional repressor (Yamaguchi et al., 2010b). The use of the VND6 promoter to perform a targeted rescue of lignification succeeded in improving saccharification, which was the goal of the study, but the authors did not comment on the role of any specific cell type in the xylem during lignification. The *CESA7* promoter, by contrast, is expressed only in cells with secondary cell walls, allowing the assessment of the role nonlignifying neighbors play during xylem lignification.

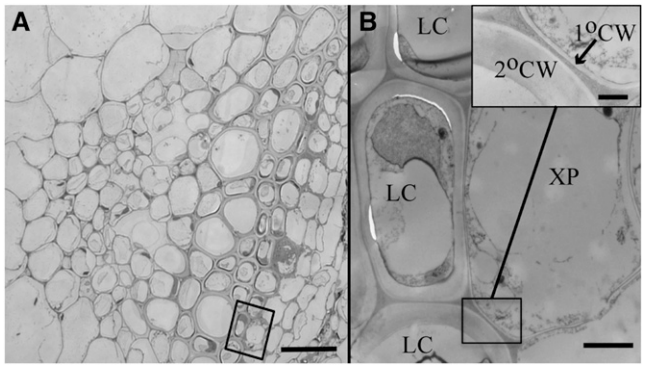

Figure 7. Anatomy of a Vascular Bundle in *Arabidopsis*.

(A) Toluidine blue–stained stem cross section showing the xylem parenchyma, tracheary elements, and xylem fiber cells. Bar = 10 μm.

(B) TEM image of xylary parenchyma cell and neighboring lignified cell (bar = 2 μm) with inset high-magnification image of boxed region showing the difference in primary and secondary cell wall thickness (bar = 500 nm).

XP, xylary parenchyma cell; LC, lignified cell; 2°CW, secondary cell wall; 1°CW, primary cell wall.

Although the focus of this study was to dissect the mechanisms of lignification by examining specifically which cells in the xylem contribute to lignification, understanding that xylary and extraxylary lignified cells employ different lignification mechanisms has implications for strategies to engineer plants with low lignin. Morphological defects common to many genetically modified plants with decreased lignin include dwarf plant stature, collapsed xylem, reduced fertility, and increased susceptibility to fungi and other pathogens (Jones et al., 2001; Schoch et al., 2001; Franke et al., 2002a, 2002b; Schilmiller et al., 2009). The *ProCESA7*:*miRNA CCR1* plants have reduced lignin levels, yet these plants grow to wild-type heights, do not have collapsed xylem and are fertile (Figure 5). Mutants with lesions in genes encoding *NAC SECONDARY WALL THICKENING PROMOTING FACTORS* (*NST*) transcription factors, such as SND1, show a similar pendant stem phenotype due to defective secondary cell wall formation in interfascicular and xylary fibers (Mitsuda et al., 2007; Zhong et al., 2007). Furthermore, *snd1/nst1* mutants do not deposit cellulose, hemicelluloses, or lignin in fiber cells (Zhong et al., 2007). The phenotype of the *ProCESA7*:*miRNA CCR1* plants is interesting from a plant engineering perspective, as it has unaffected xylem lignification, yet reduced overall lignin content. This phenotype was deliberately engineered by Yang et al. (2013) and demonstrated to have improved saccharification. The extraxylary fiber cells, which displayed reduced lignin in this study, make a substantial contribution to plant biomass, especially in potential biofuel feedstock taxa such as the grasses. There would therefore appear to be opportunities for independently manipulating two lignin pools, xylary and extraxylary, to create plants with intact xylem but overall lower lignin levels.

METHODS

Plant Growth Conditions and Staining/Phenylpropanoid Radiolabeling

Arabidopsis thaliana (Columbia-0 [Col-0]) seeds were grown on half-strength Murashige and Skoog media (Sigma-Aldrich) under continuous light until seedlings were 7 d old and then seedling roots were used for histochemical staining. Whole seedlings were stained in 0.0001% Basic fuchsin in 95% ethanol for 5 min, followed by destaining for 2 min in 70% ethanol. Seedlings were mounted in 50% glycerol, and the lignin fluorescence in roots was observed using a Leica DMR light microscope using a red filter set (excitation 560 nm; emission 645 nm). Images were captured using a Q-CAM digital camera (Q-Imaging). Seedlings were grown in a growth chamber at 21°C under 16/8-h light/dark cycles. Plant inflorescence stems were destructively sampled after 2 months, and thin hand sections were taken from the base of the stem. Sections were stained with phloroglucinol-HCl for 5 min, mounted in water, and analyzed using bright-field microscopy (Leica DMR microscope).

For autoradiography of seedling roots, 7-d-old seedlings were placed in a solution containing 0.25 mL of 0.2 M Suc and 12.5 μCi of L-[2,6-^{3}H]Phe (0.9 μM Phe; GE Healthcare) in 2-mL Eppendorf tubes and incubated at room temperature for 2 h. Separate treatments were set up containing ^{3}H-Phe with or without 10 μM cycloheximide (Sigma-Aldrich) or 10 μM piperonylic acid (Sigma-Aldrich). After the 2-h incubation, the samples were high-pressure frozen for subsequent sectioning and autoradiography.

High-Pressure Freezing

Seedling roots were high-pressure frozen in 1-hexadecene (as a cryoprotectant) using a Leica EM HPM 100 high-pressure freezer. Samples were freeze substituted with 2% osmium tetroxide in 8% dimethoxypropane in acetone for 120 h in a dry ice-acetone bath at approximately −80°C as previously described (Young et al., 2008). Acetone was gradually replaced with Spurr's resin (Spurr, 1969). Samples were embedded in fresh Spurr's resin in flat-bottomed beam capsules and allowed to polymerize overnight at 60°C. Extraction of radiolabel during fixation and embedding was assessed by collecting 50 to 100 μL of the fixative or resin solution, adding it to 3 mL of Fisher ScintiVerse scintillation cocktail, and counting the number of decay events per minute in a Beckman LS600IC liquid scintillation counter.

Autoradiography and Light Microscopy

Sections (300 to 350 nm) were made using a Leica Ultracut microtome and heat-fixed onto glass slides. To control for differences in emulsion thickness and to facilitate comparison between treatments, sections from both ^{3}H-Phe and ^{3}H-Phe plus cycloheximide samples were placed on the same slides. For every three sections prepared for autoradiography, one section was placed on a separate glass slide and stained with 1% Toluidine Blue-O in 1% sodium borate as a reference for the autoradiography sections. Slides for autoradiography were dipped in a 50% (v/v) aqueous solution of Ilford L4 emulsion (PolySciences) at 40°C under a sodium safelight with closed filters (Thomas Duplex Super Safelight). Dipped slides were stored in a light-proof box at 4°C for 2 d. The emulsions were developed in Kodak D19 developer solution (1:1 dilution in water) for 5 min, rinsed in distilled water, fixed in a 10% (v/v) aqueous solution of Ilford Multigrade Paper Fixer, and gently rinsed under cold running water for 15 min. The autoradiographs, and the Toluidine Blue–stained reference sections, were mounted in 50% glycerol and observed using a Leica DMR light microscope and Q-CAM digital camera (Q-Imaging).

TEM

Thin sections (70 to 75 nm) were made on a Leica Ultracut microtome using a diamond knife and placed on copper Athene polyslot grids (Canemco) coated with 0.3% Formvar in 1,2-dichloroethane. The grids were stained for 20 min with 2% uranyl acetate (w/v) in 70% methanol and 5 min with Reynold's lead citrate and then were carbon coated (Bal-Tec MED 010 evaporator and glow discharge apparatus). Reference grids remained uncoated and were examined and photographed using a Hitachi H7600 transmission electron microscope with AMT Advantage charge-coupled device camera. Under a sodium safe-light, 7-mm-diameter wire loops were dipped in 1:1.7 Ilford L4 emulsion:distilled water solutions at 40°C and placed horizontally until almost dried, and then stained and carbon-coated autoradiography grids were placed sample side down on the emulsion. The emulsion was allowed to dry completely before the grid plus emulsion were removed from the loop, placed in a grid box, wrapped in aluminum foil, and placed in a light-tight photographic storage bag. Grids were stored at 4°C for 2 to 3 weeks before emulsion development. Emulsions were developed as described above for light microscopy thick sections.

Confocal Imaging

Live-cell imaging of *ProCESA7*:*GFP* and *ProUBQ10*:*YFP-CCR1* plants was performed on a Perkin-Elmer UltraView VoX spinning disk confocal mounted on a Leica DMI6000 inverted microscope using a Hamamatsu 9100-02 charge-coupled device camera with the following excitation/emission filters: GFP (488/525) and YFP (514/540). For imaging *YFP-CCR1*, or *ProCESA7*:*GFP*, 7-d-old seedlings were mounted in half-strength Murashige and Skoog solution on slides and imaged using Leica oil immersion ×63 or ×20 objectives. All images were captured and processed using Volocity image analysis software (Improvision).

Transgenic Lines

Gateway cloning technology (Invitrogen) was used to generate the following constructs related to *CESA7/IRX3* and *CCR1*. *ProCESA7*:*GFP* (*pMDC107*; Curtis and Grossniklaus, 2003) was generated using 1127 bp upstream of the transcriptional start site of *CESA7*. The other Gateway constructs generated were *Pro35S*:*miRNA CCR*, *ProCESA7*:*miRNA CCR* (*pK2GW7* and *pKGW*, respectively; Karimi et al., 2002), and *ProUBQ10*:*YFP-CCR1* (pUBN:YFP; Grefen et al., 2010) (primers are listed in Supplemental Table 2 online). Artificial microRNAs were designed using the Web microRNA designer (http://wmd2.weigelworld.org) and amplified using primers listed in Supplemental Table 2 online and as described by Schwab et al. (2006). Plant expression constructs were introduced into *Agrobacterium tumefaciens* strain GV3101 and transformed into *Arabidopsis* Col-0 using the floral dip method (Clough and Bent, 1998) to generate transgenic plants.

Quantitative RT-PCR

RNA extraction was performed using TRIzol (Invitrogen) after grinding 6-week-old *Arabidopsis* stems in liquid nitrogen. RNA was quantified using a Nanodrop spectrophotometer (Thermo Fisher Scientific), and cDNA was generated using SuperScript III reverse transcriptase (Invitrogen) and oligo (dT) primers as per the manufacturers' instructions. Quantitative RT-PCR was performed using IQ SYBR Green supermix (Bio-Rad) and cycled using a CFX Connect real-time system (Bio-Rad) according to the manufacturer's specifications. Relative gene expression was calculated using the $\Delta\Delta$ cycle threshold method (Livak and Schmittgen, 2001).

Chemical Analysis

Dried *Arabidopsis* stems (the wild type, *Pro35S*:*miRNA CCR*, and *ProCESA7*:*miRNA CCR*) were ground to a fine powder using a mortar and pestle or a Wiley mill coupled to a 40 mesh screen. Extractive-free tissue powder was generated by acetone extraction for 7 to 16 h followed by drying at 50°C overnight. Extractive-free tissue (10 mg) was used to determine relative guaiacyl and syringyl monolignol abundance using thioacidolysis (Robinson and Mansfield, 2009) with tetracosane (200 μL at a concentration of 5 mg/mL methylene chloride) as the internal standard. Gas chromatography was performed on a ThermoFinnigan Trace GC-PolarisQ instrument equipped with a DB-5 column, as previously described (Coleman et al., 2008). Acid-insoluble lignin was determined using Klason lignin analysis of 200 mg of extractive-free tissue, as previously described (Coleman et al., 2008). Acid-soluble lignin was determined by measuring the absorbance of the filtrate after isolation of acid insoluble lignin at 205 nm and calculated using an extinction coefficient of 110 L/g-cm.

Accession Numbers

Sequence data from this article can be found in the Arabidopsis Genome Initiative or GenBank/EMBL databases under the following accession numbers: *CESA7*, AT5G17420; and *CCR1*, AT1G15950.

Supplemental Data

The following materials are available in the online version of this article.

Supplemental Figure 1. Characterization of ^{3}H-Phe–Treated Roots.

Supplemental Figure 2. Localization of *ProCESA7*:*GFP* in Inflorescence Stems of *Arabidopsis*.

Supplemental Figure 3. CCR1 miRNA Effectively Silences *YFP-CCR1* Expression.

Supplemental Figure 4. CCR1 miRNA Silences YFP-CCR1 Expression Only in Lignified Cells in the Stem.

Supplemental Figure 5. RT-PCR Results for *CCR1* Expression Level in the Stems of miRNA Lines.

Supplemental Table 1. Lignin Monomer Content Analysis of Different miRNA Lines.

Supplemental Table 2. Primer Sequences.

ACKNOWLEDGMENTS

We thank the University of British Columbia Bioimaging Facility and the Canadian Natural Sciences and Engineering Research Council for Discovery and CREATE grants to B.E., S.D.M., and L.S. We also thank Foster Hart for technical assistance.

AUTHOR CONTRIBUTIONS

R.A.S., M.S., B.E., and L.S. designed the research. R.A.S. and M.S. performed the research. M.R. and S.D.M. provided analytical tools. All authors analyzed the data and wrote the article.

Received August 8, 2013; revised September 9, 2013; accepted September 17, 2013; published October 4, 2013.

REFERENCES

Alejandro, S., Lee, Y., Tohge, T., Sudre, D., Osorio, S., Park, J., Bovet, L., Lee, Y., Geldner, N., Fernie, A.R., and Martinoia, E. (2012). AtABCG29 is a monolignol transporter involved in lignin biosynthesis. Curr. Biol. **22:** 1207–1212.

Baghdady, A., Blervacq, A.S., Jouanin, L., Grima-Pettenati, J., Sivadon, P., and Hawkins, S. (2006). *Eucalyptus gunnii CCR* and *CAD2* promoters are active in lignifying cells during primary and secondary xylem formation in *Arabidopsis thaliana*. Plant Physiol. Biochem. **44:** 674–683.

Bednarek, P., Schneider, B., Svatos, A., Oldham, N.J., and Hahlbrock, K. (2005). Structural complexity, differential response to infection, and tissue specificity of indolic and phenylpropanoid secondary metabolism in Arabidopsis roots. Plant Physiol. **138:** 1058–1070.

Berthet, S., Demont-Caulet, N., Pollet, B., Bidzinski, P., Cézard, L., Le Bris, P., Borrega, N., Hervé, J., Blondet, E., Balzergue, S., Lapierre, C., and Jouanin, L. (2011). Disruption of *LACCASE4* and *17* results in tissue-specific alterations to lignification of *Arabidopsis thaliana* stems. Plant Cell **23:** 1124–1137.

Bevan, M., Shufflebottom, D., Edwards, K., Jefferson, R., and Schuch, W. (1989). Tissue- and cell-specific activity of a phenylalanine ammonia-lyase promoter in transgenic plants. EMBO J. **8:** 1899–1906.

Chapelle, A., Morreel, K., Vanholme, R., Le-Bris, P., Morin, H., Lapierre, C., Boerjan, W., Jouanin, L., and Demont-Caulet, N. (2012). Impact of the absence of stem-specific β-glucosidases on lignin and monolignols. Plant Physiol. **160:** 1204–1217.

Chen, C., Meyermans, H., Burggraeve, B., De Rycke, R.M., Inoue, K., De Vleesschauwer, V., Steenackers, M., Van Montagu, M.C., Engler, G.J., and Boerjan, W.A. (2000). Cell-specific and conditional expression of caffeoyl-coenzyme A-3-O-methyltransferase in poplar. Plant Physiol. **123:** 853–867.

Chong, J., Pierrel, M.A., Atanassova, R., Werck-Reichhart, D., Fritig, B., and Saindrenan, P. (2001). Free and conjugated benzoic acid in tobacco plants and cell cultures. Induced accumulation

upon elicitation of defense responses and role as salicylic acid precursors. Plant Physiol. **125:** 318–328.

Clough, S.J., and Bent, A.F. (1998). Floral dip: A simplified method for *Agrobacterium*-mediated transformation of *Arabidopsis thaliana*. Plant J. **16:** 735–743.

Coleman, H.D., Park, J.Y., Nair, R., Chapple, C., and Mansfield, S.D. (2008). RNAi-mediated suppression of *p*-coumaroyl-CoA 3′-hydroxylase in hybrid poplar impacts lignin deposition and soluble secondary metabolism. Proc. Natl. Acad. Sci. USA **105:** 4501–4506.

Courtois-Moreau, C.L., Pesquet, E., Sjödin, A., Muñiz, L., Bollhöner, B., Kaneda, M., Samuels, L., Jansson, S., and Tuominen, H. (2009). A unique program for cell death in xylem fibers of *Populus* stem. Plant J. **58:** 260–274.

Curtis, M.D., and Grossniklaus, U. (2003). A Gateway cloning vector set for high-throughput functional analysis of genes *in planta*. Plant Physiol. **133:** 462–469.

Feuillet, C., Lauvergeat, V., Deswarte, C., Pilate, G., Boudet, A., and Grima-Pettenati, J. (1995). Tissue- and cell-specific expression of a cinnamyl alcohol dehydrogenase promoter in transgenic poplar plants. Plant Mol. Biol. **27:** 651–667.

Franke, R., Hemm, M.R., Denault, J.W., Ruegger, M.O., Humphreys, J.M., and Chapple, C. (2002a). Changes in secondary metabolism and deposition of an unusual lignin in the *ref8* mutant of *Arabidopsis*. Plant J. **30:** 47–59.

Franke, R., Humphreys, J.M., Hemm, M.R., Denault, J.W., Ruegger, M.O., Cusumano, J.C., and Chapple, C. (2002b). The *Arabidopsis REF8* gene encodes the 3-hydroxylase of phenylpropanoid metabolism. Plant J. **30:** 33–45.

Gorzsás, A., Stenlund, H., Persson, P., Trygg, J., and Sundberg, B. (2011). Cell-specific chemotyping and multivariate imaging by combined FT-IR microspectroscopy and orthogonal projections to latent structures (OPLS) analysis reveals the chemical landscape of secondary xylem. Plant J. **66:** 903–914.

Grefen, C., Donald, N., Hashimoto, K., Kudla, J., Schumacher, K., and Blatt, M.R. (2010). A ubiquitin-10 promoter-based vector set for fluorescent protein tagging facilitates temporal stability and native protein distribution in transient and stable expression studies. Plant J. **64:** 355–365.

Hauffe, K.D., Paszkowski, U., Schulze-Lefert, P., Hahlbrock, K., Dangl, J.L., and Douglas, C.J. (1991). A parsley 4CL-1 promoter fragment specifies complex expression patterns in transgenic tobacco. Plant Cell **3:** 435–443.

Hemm, M.R., Rider, S.D., Ogas, J., Murry, D.J., and Chapple, C. (2004). Light induces phenylpropanoid metabolism in *Arabidopsis* roots. Plant J. **38:** 765–778.

Hosokawa, M., Suzuki, S., Umezawa, T., and Sato, Y. (2001). Progress of lignification mediated by intercellular transportation of monolignols during tracheary element differentiation of isolated Zinnia mesophyll cells. Plant Cell Physiol. **42:** 959–968.

Humphreys, J.M., and Chapple, C. (2002). Rewriting the lignin roadmap. Curr. Opin. Plant Biol. **5:** 224–229.

Jones, L., Ennos, A.R., and Turner, S.R. (2001). Cloning and characterization of *irregular xylem4* (*irx4*): A severely lignin-deficient mutant of *Arabidopsis*. Plant J. **26:** 205–216.

Kaneda, M., Rensing, K.H., Wong, J.C.T., Banno, B., Mansfield, S.D., and Samuels, A.L. (2008). Tracking monolignols during wood development in lodgepole pine. Plant Physiol. **147:** 1750–1760.

Karimi, M., Inzé, D., and Depicker, A. (2002). GATEWAY vectors for Agrobacterium-mediated plant transformation. Trends Plant Sci. **7:** 193–195.

Kubo, M., Udagawa, M., Nishikubo, N., Horiguchi, G., Yamaguchi, M., Ito, J., Mimura, T., Fukuda, H., and Demura, T. (2005). Transcription switches for protoxylem and metaxylem vessel formation. Genes Dev. **19:** 1855–1860.

Lanot, A., Hodge, D., Jackson, R.G., George, G.L., Elias, L., Lim, E.K., Vaistij, F.E., and Bowles, D.J. (2006). The glucosyltransferase UGT72E2 is responsible for monolignol 4-O-glucoside production in *Arabidopsis thaliana*. Plant J. **48:** 286–295.

Lee, Y., Rubio, M.C., Alassimone, J., and Geldner, N. (2013). A mechanism for localized lignin deposition in the endodermis. Cell **153:** 402–412.

Leinhos, V., and Savidge, R.A. (1993). Isolation of protoplasts from developing xylem of *Pinus banksiana* and *Pinus strobus*. Can. J. For. Res. **23:** 343–348.

Liu, C.J., Miao, Y.C., and Zhang, K.W. (2011). Sequestration and transport of lignin monomeric precursors. Molecules **16:** 710–727.

Livak, K.J., and Schmittgen, T.D. (2001). Analysis of relative gene expression data using real-time quantitative PCR and the 2(-Delta Delta C(T)) method. Methods **25:** 402–408.

McDonnell, L.M. (2010). Investigating the Role of Cellulose Synthases in the Biosynthesis and Properties of Cellulose in Secondary Cell Walls. PhD dissertation (Vancouver, Canada: University of British Columbia).

Miao, Y.C., and Liu, C.J. (2010). ATP-binding cassette-like transporters are involved in the transport of lignin precursors across plasma and vacuolar membranes. Proc. Natl. Acad. Sci. USA **107:** 22728–22733.

Mir Derikvand, M., Sierra, J.B., Ruel, K., Pollet, B., Do, C.T., Thévenin, J., Buffard, D., Jouanin, L., and Lapierre, C. (2008). Redirection of the phenylpropanoid pathway to feruloyl malate in *Arabidopsis* mutants deficient for cinnamoyl-CoA reductase 1. Planta **227:** 943–956.

Mitsuda, N., Iwase, A., Yamamoto, H., Yoshida, M., Seki, M., Shinozaki, K., and Ohme-Takagi, M. (2007). NAC transcription factors, NST1 and NST3, are key regulators of the formation of secondary walls in woody tissues of *Arabidopsis*. Plant Cell **19:** 270–280.

Naseer, S., Lee, Y., Lapierre, C., Franke, R., Nawrath, C., and Geldner, N. (2012). Casparian strip diffusion barrier in *Arabidopsis* is made of a lignin polymer without suberin. Proc. Natl. Acad. Sci. USA **109:** 10101–10106.

Ossowski, S., Schwab, R., and Weigel, D. (2008). Gene silencing in plants using artificial microRNAs and other small RNAs. Plant J. **53:** 674–690.

Pesquet, E., Korolev, A.V., Calder, G., and Lloyd, C.W. (2010). The microtubule-associated protein AtMAP70-5 regulates secondary wall patterning in *Arabidopsis* wood cells. Curr. Biol. **20:** 744–749.

Pesquet, E., et al. (2013). Non-cell-autonomous postmortem lignification of tracheary elements in *Zinnia elegans*. Plant Cell **25:** 1314–1328.

Pickett-Heaps, J.D. (1968). Radiographic investigations using lignin precursors. Protoplasma **65:** 181–205.

Roberts, A.W., Frost, A.O., Roberts, E.M., and Haigler, C.H. (2004). Roles of microtubules and cellulose microfibril assembly in the localization of secondary-cell-wall deposition in developing tracheary elements. Protoplasma **224:** 217–229.

Robinson, A.R., and Mansfield, S.D. (2009). Rapid analysis of poplar lignin monomer composition by a streamlined thioacidolysis procedure and near-infrared reflectance-based prediction modeling. Plant J. **58:** 706–714.

Schilmiller, A.L., Stout, J., Weng, J.K., Humphreys, J., Ruegger, M.O., and Chapple, C. (2009). Mutations in the cinnamate 4-hydroxylase gene impact metabolism, growth and development in *Arabidopsis*. Plant J. **60:** 771–782.

Schoch, G., Goepfert, S., Morant, M., Hehn, A., Meyer, D., Ullmann, P., and Werck-Reichhart, D. (2001). CYP98A3 from *Arabidopsis thaliana* is a 3′-hydroxylase of phenolic esters, a missing link in the phenylpropanoid pathway. J. Biol. Chem. **276:** 36566–36574.

Schwab, R., Ossowski, S., Riester, M., Warthmann, N., and Weigel, D. (2006). Highly specific gene silencing by artificial microRNAs in *Arabidopsis*. Plant Cell **18:** 1121–1133.

Sibout, R., and Höfte, H. (2012). Plant cell biology: The ABC of monolignol transport. Curr. Biol. **22:** R533–R535.

Takabe, K., Fujita, M., Harada, H., and Saiki, H. (1985). Autoradiographic investigation of lignification in the cell walls of Cryptomeria (*Cryptomeria Japonica* D Don). Mokuzai Gakkaishi **31:** 613–619.

Taylor, N.G., Howells, R.M., Huttly, A.K., Vickers, K., and Turner, S.R. (2003). Interactions among three distinct CesA proteins essential for cellulose synthesis. Proc. Natl. Acad. Sci. USA **100:** 1450–1455.

Taylor, N.G., Scheible, W.R., Cutler, S., Somerville, C.R., and Turner, S.R. (1999). The *irregular xylem3* locus of *Arabidopsis* encodes a cellulose synthase required for secondary cell wall synthesis. Plant Cell **11:** 769–780.

Terashima, N., Fukushima, K., He, L., and Takabe, K. (1993). Comprehensive model of the lignified plant cell wall. In Forage Cell Wall Structure and Digestibility, H.G. Jung, D.R. Buxton, R.D. Hatfield, and J. Ralph, eds (Madison, WI: ASA, CSSA, and SSSA), pp. 247–270.

Terashima, N., Fukushima, K., and Takabe, K. (1986). Heterogeneity in formation of lignin. VIII. An autoradiographic study on the formation of guaiacyl and syringyl lignin in *Magnolia Kobus* DC. Wood Sci. Technol. **40:** 101–105.

Terashima, N., and Fukushima, K. (1988). Heterogeneity in formation of lignin. XI. An autoradiographic study of the heterogeneous formation and structure of pine lignin. Wood Sci. Technol. **22:** 259–270.

Thévenin, J., Pollet, B., Letarnec, B., Saulnier, L., Gissot, L., Maia-Grondard, A., Lapierre, C., and Jouanin, L. (2011). The simultaneous repression of CCR and CAD, two enzymes of the lignin biosynthetic pathway, results in sterility and dwarfism in *Arabidopsis thaliana*. Mol. Plant **4:** 70–82.

Tokunaga, N., Sakakibara, N., Umezawa, T., Ito, Y., Fukuda, H., and Sato, Y. (2005). Involvement of extracellular dilignols in lignification during tracheary element differentiation of isolated Zinnia mesophyll cells. Plant Cell Physiol. **46:** 224–232.

Turner, S.R., and Somerville, C.R. (1997). Collapsed xylem phenotype of *Arabidopsis* identifies mutants deficient in cellulose deposition in the secondary cell wall. Plant Cell **9:** 689–701.

Vanholme, R., Demedts, B., Morreel, K., Ralph, J., and Boerjan, W. (2010). Lignin biosynthesis and structure. Plant Physiol. **153:** 895–905.

Yamaguchi, M., Goué, N., Igarashi, H., Ohtani, M., Nakano, Y., Mortimer, J.C., Nishikubo, N., Kubo, M., Katayama, Y., Kakegawa, K., Dupree, P., and Demura, T. (2010a). VASCULAR-RELATED NAC-DOMAIN6 and VASCULAR-RELATED NAC-DOMAIN7 effectively induce transdifferentiation into xylem vessel elements under control of an induction system. Plant Physiol. **153:** 906–914.

Yamaguchi, M., Ohtani, M., Mitsuda, N., Kubo, M., Ohme-Takagi, M., Fukuda, H., and Demura, T. (2010b). VND-INTERACTING2, a NAC domain transcription factor, negatively regulates xylem vessel formation in *Arabidopsis*. Plant Cell **22:** 1249–1263.

Yang, F., Mitra, P., Zhang, L., Prak, L., Verhertbruggen, Y., Kim, J.S., Sun, L., Zheng, K., Tang, K., Auer, M., Scheller, H.V., and Loqué, D. (2013). Engineering secondary cell wall deposition in plants. Plant Biotechnol. J. **11:** 325–335.

Young, R.E., McFarlane, H.E., Hahn, M.G., Western, T.L., Haughn, G.W., and Samuels, A.L. (2008). Analysis of the Golgi apparatus in *Arabidopsis* seed coat cells during polarized secretion of pectin-rich mucilage. Plant Cell **20:** 1623–1638.

Zhong, R., Lee, C., and Ye, Z.H. (2010). Evolutionary conservation of the transcriptional network regulating secondary cell wall biosynthesis. Trends Plant Sci. **15:** 625–632.

Zhong, R., Richardson, E.A., and Ye, Z.H. (2007). Two NAC domain transcription factors, SND1 and NST1, function redundantly in regulation of secondary wall synthesis in fibers of *Arabidopsis*. Planta **225:** 1603–1611.